

Global and multiscale aspects of magnetospheric dynamics in local-linear filters

A. Y. Ukhorskiy, M. I. Sitnov, A. S. Sharma, and K. Papadopoulos

Department of Physics, University of Maryland at College Park, College Park, Maryland, USA

Received 6 November 2001; revised 23 May 2002; accepted 10 July 2002; published 16 November 2002.

[1] The magnetospheric dynamics consists of global and multiscale components. The local-linear filters (LLFs) relating the solar wind input and the magnetospheric output have been used earlier to predict the global dynamical behavior. In this paper, the relative role of global and multiscale processes in the prediction of magnetospheric dynamics is studied. The filters are derived from the reconstructed input–output magnetospheric phase space using time series of VB_S as the input and AL index as the output. We show that the conventional formula for the LLF can be broken into two parts corresponding to the global and multiscale constituents. The first part is the zeroth-order term, which is obtained by the phase space average of the model outputs. This is a feature similar to the mean-field model in phase transition physics, which yields iterative predictions of the global coherent component. The second part consists of the higher-order terms of the filter, which are highly irregular and thus cannot be used in dynamical prediction. This irregular behavior represents the departure from the low-dimensional dynamics underlying earlier studies using LLFs. The earlier prediction studies mixed these two components. However, by separating these two components, the prediction procedure is highly simplified and longer period predictions are achieved. The multiscale nature arises from the perturbations over a wide range of scales and has a power spectrum similar to that of colored noise. When these perturbations are taken into account in the prediction process, the iterative predictions yield a factor of four improvement in the accuracy compared to the mean-field model. However, the filter technique does not provide a prescription for correctly including the multiscale aspects in a dynamical model and further improvement in forecasting can be achieved by a statistical approach. These results have important implications for space weather forecasting. *INDEX TERMS*: 2139 Interplanetary Physics: Interplanetary shocks; 2164 Interplanetary Physics: Solar wind plasma; 2102 Interplanetary Physics: Corotating streams; 2111 Interplanetary Physics: Ejecta, driver gases, and magnetic clouds; 7513 Solar Physics, Astrophysics, and Astronomy: Coronal mass ejections; *KEYWORDS*: magnetosphere, substorm, chaos, filters, phase transitions, SOC

Citation: Ukhorskiy, A. Y., M. I. Sitnov, A. S. Sharma, and K. Papadopoulos, Global and multiscale aspects of magnetospheric dynamics in local-linear filters, *J. Geophys. Res.*, 107(A11), 1369, doi:10.1029/2001JA009160, 2002.

1. Introduction

[2] The solar wind energy penetrates into the magnetosphere by magnetic field line reconnection at the dayside magnetopause, giving rise to magnetospheric substorms. Due to the imbalance between the reconnection rate on the dayside magnetopause and at the distant neutral line a fraction of the solar wind energy is accumulated in the magnetotail, mainly in the form of magnetic energy, and is then suddenly released. Substorms have a variety of distinct manifestations in the ionosphere (magnetic field perturbations at the polar regions, auroral brightening, particle precipitation) as well as in the mid and distant magnetotail (plasmoid formation and ejection). Magnetospheric activity

during substorms extends from small-scale processes, such as pseudobreakups, MHD turbulence, and current disruption, to large-scale processes, such as global convection, field line depolarization, and plasmoid ejection. Thus, the magnetosphere behaves as a nonlinear, open, spatially extended system, which on the one hand is well organized on global scale and on the other hand exhibits activity over a wide range of spatial and temporal scales.

[3] There has been a considerable progress in the modeling and understanding the solar wind–magnetosphere coupling using nonlinear dynamical techniques. In this approach the system evolution is described directly from data, using special techniques such as time delay embedding, singular spectrum analyses, linear and local-linear filters (LLFs) [Sharma *et al.*, 1993; Sharma, 1995; Vassiliadis *et al.*, 1995]. The clear advantage of data-derived models is their ability to reveal inherent features of dynamics even in the

presence of complexity and strong nonlinearity. The earlier dynamical models of the magnetospheric activity were motivated by the global coherence indicated by the geomagnetic indices and inspired by the concept of dynamical chaos. They were based on the assumption that the observed complexity of the system is mainly attributed to the nonlinear dynamics of a few dominant degrees of freedom [Sharma, 1995; Klimas et al., 1996]. Studies of the magnetosphere as a dynamical system using modern techniques of data processing and phase space reconstruction [Grassberger and Procaccia, 1983; Abarbanel et al., 1993] based on AE index time series gave evidences of low effective dimension of the magnetosphere [Vassiliadis et al., 1990; Sharma et al., 1993]. Further elaboration of this hypothesis resulted in creating space weather forecasting tools based on LLF with autoregression [Price et al., 1994; Vassiliadis et al., 1995; Sharma, 1995] and data-derived analogues [Klimas et al., 1992]. The low-dimensional organized behavior of the magnetosphere during substorms is also evident in many spacecraft in situ observations including the INTERBALL and GEOTAIL missions [Jeda et al., 1998; Nagai et al., 1998; Petrukovich et al., 1998]. These studies confirm such key features of the globally coherent dynamics as plasmoid ejection, field line dipolarization, generation of hot earthward plasma flows, etc.

[4] However subsequent studies have shown that not all aspects of magnetospheric dynamics during substorms conform to the hypothesis of low dimensionality and thus cannot be accounted within the framework of dynamical chaos and self-organization. For example, the power spectrum of AE index data [Tsurutani et al., 1990] and magnetic field fluctuations in the tail current sheet [Ohtani et al., 1995] have a power law form typical for high-dimensional colored noise. Prichard and Price [1992] have argued that using a modified correlation integral [Theiler, 1991] a low correlation dimension cannot be found for the magnetospheric dynamics. Moreover, detailed analyses [Takalo et al., 1993, 1994] have shown that the qualitative properties of the AE time series are much more similar to bicolored noise than to the time series generated by low-dimensional chaotic systems. One interpretation of these multiscale aspects of magnetospheric dynamics was suggested to be a multifractal behavior generated by intermittent turbulence [Consolini et al., 1996; Borovsky et al., 1997; Chang, 1998; Angelopoulos et al., 1999]. Another popular approach to magnetosphere modeling is based on the concept of self-organized criticality (SOC) [Bak et al., 1987]. SOC explicitly takes into account the large number of degrees of freedom and the interactions among them on different scales. According to SOC models [Consolini, 1997; Chapman et al., 1998; Uritsky and Pudovkin, 1998; Chang, 1999; Takalo et al., 1999; Watkins et al., 1999; Klimas et al., 2000] multiscale behavior arises spontaneously and requires no tuning of the system parameters, in other words SOC is attractor of dynamics.

[5] Although SOC can account for the characteristic power spectra observed in a number of processes during substorms it is doubtful that SOC alone can provide the framework for modeling the solar wind–magnetosphere coupling. Indeed, it turns out that SOC, which was developed to model sand pile behavior, is oversimplified even for modeling real sand piles [Nagel, 1992]. Violations of SOC

behavior were detected in observations of particle injections in the near-Earth magnetosphere [Borovsky et al., 1993; Prichard et al., 1996] and substorm chorus events [Smith et al., 1996]. Besides, the magnetosphere is essentially nonautonomous with dynamics governed to a large extent by the external driver, the solar wind, while in SOC the criticality is reached by a fine tuning of the control parameter (i.e., driving rate) to the vanishing value [Vespignani and Zapperi, 1998]. Some models that internally exhibit SOC can simultaneously generate non-SOC global instabilities [Chapman et al., 1998]. However, since such system-wide avalanches were found only in the simplified sand pile models, this still cannot account for the specific coherent features of the actual magnetospheric dynamics. Moreover, since the fluctuations of the system at a critical point are completely uncorrelated it removes the possibility of even short-term predictability of the system's evolution while it was clearly demonstrated [Sharma, 1995; Vassiliadis et al., 1995; Valdivia et al., 1996] that input–output models yield good predictions of global magnetospheric activity.

[6] One of the ways to reconcile global and multiscale aspects of dynamics in unified model is suggested by the physics of phase transitions. There are two different types of phase transitions, which are intimately related to each other and naturally coexist in a single system. The first-order phase transitions are characterized by a low-dimensional manifold in the phase space, e.g., the temperature–pressure–density surface for water–steam transitions. In first-order phase transitions the first derivative of the state parameter of the system like density in water–steam transition or magnetization in ferromagnets is discontinuous. The distinctive feature of second-order phase transitions, which represent the behavior of the system at criticality (i.e., in the vicinity of the singular point of the phase transition surface), is their scale invariance reflected by various power law spectra and critical exponents [Stanley, 1971]. Phase transitions in real nonautonomous systems are essentially dynamic and are nonequilibrium which results in additional properties like hysteresis and dynamical critical exponents [Hohenberg and Halperin, 1977; Chakrabarti and Acharyya, 1999; Zheng et al., 1999]. It has been noted [Sitnov et al., 2000, 2001; Sharma et al., 2001] that the magnetospheric dynamics during substorms shares a number of properties with nonequilibrium phase transitions. In particular, it was shown that multiscale substorm activity resembles second-order phase transitions, while the large-scale perturbations reveal the features of first-order nonequilibrium transitions including hysteresis and global structure similar to the “temperature–pressure–density” diagram. Although the phase transition analogy gives an insight into various properties of the magnetospheric dynamics its implications to the forecasting of magnetospheric evolution are not clear yet.

[7] The main purpose of the paper is to study the role of multiscale processes in the prediction of magnetospheric dynamics. The multiscale processes have been ignored in the earlier studies and this has limited the quality of the predictions. The LLFs relating the solar wind input and the magnetospheric output are used to analyze the relative roles of global and multiscale constituents of the magnetospheric behavior during substorms.

[8] It is found that in spite of the low dimensionality assumption that lies underneath the LLF model, filters are

still capable of mimicking the multiscale high-dimensional component of magnetospheric dynamics. We show that the conventional formula for LLF can be broken into two parts, which are responsible for different dynamical constituents. The first part, the zeroth-order term of LLF, is the phase space average of the model outputs, which is similar to the mean-field model in phase transitions. It yields iterative predictions of AL dynamics naturally separating the global coherent component from the time series. We also show that the second part, which consists of the higher-order terms of the filter, is irregular and thus is irrelevant for predictions. This irregular behavior indicates the fundamental difference between low-dimensional scale-invariant dynamic systems like Lorenz attractor and the magnetosphere, which does not possess low dimensionality on smaller scales. Nevertheless, the higher-order terms in the filter formula still can model multiscale constituents of the magnetospheric dynamics, whose properties, both statistical and dynamical are very similar to those of systems at criticality.

[9] The next section describes the LLFs and how they represent the global and multiscale features of the solar wind–magnetosphere system. In section 4 the predictions of the global magnetospheric dynamics using the center of mass component of LLF is discussed. The multiscale aspects modeled in section 5 by data reconstruction, and this yields an estimate of the complexity in terms of the dimensionality of the space needed to represent the system. The last section presents the main results of the paper and their implications to space weather forecasting.

2. Time Delay Embedding, Center of Mass, and LLFs

[10] In this section we discuss the primary aspects of constructing a dynamical model of nonautonomous (input–output) system based on LLFs with autoregression [Abarbanel *et al.*, 1993; Sauer, 1993; Vassiliadis *et al.*, 1995]. In this model a scalar time series $I(t)$ is used as the input which yields the output of the model $O(t)$.

[11] It is assumed that the scalar time series data of observable quantities is a function only of the state of the underlying system and contains all the information necessary to determine its evolution. Thus, if a space large enough to unfold the dynamical attractor is reconstructed from the time series and the present state of the system is identified, then the information about the future can be inferred from the known evolution of similar states.

[12] For nonlinear dynamical models the phase space of the system is reconstructed first using the time delay embedding method [Packard *et al.*, 1980; Takens, 1981; Broomhead and King, 1986; Sauer *et al.*, 1991]. The embedding theorem [Takens, 1981] states that in the absence of noise, if $M \geq 2N + 1$, then M -dimensional delay vectors generically form an embedding of the underlying phase space of the N -dimensional dynamical system. Although Takens theorem is strictly valid for autonomous systems only, numerous studies [e.g., Casdagli, 1992; Sharma, 1995; Vassiliadis *et al.*, 1995; Sitnov *et al.*, 2000] have used successfully the delay embedding method for modeling nonautonomous dynamical systems. In this

case the M -dimensional embedding space is formed by input–output delay vectors:

$$\begin{aligned} \bar{\mathbf{x}}_n &= (\bar{\mathbf{I}}_n, \bar{\mathbf{O}}_n)^T \\ &= (\mathbf{I}_n, \mathbf{I}_{n-1}, \dots, \mathbf{I}_{n-(M_i-1)}, \mathbf{O}_n, \mathbf{O}_{n-1}, \dots, \mathbf{O}_{n-(M_o-1)})^T \end{aligned} \quad (1)$$

where $\mathbf{I}_n = \mathbf{I}(t_0 + n \cdot \tau)$, $\mathbf{O}_n = \mathbf{O}(t_0 + n \cdot \tau)$, τ is the delay time, $M_i + M_o = M$. If the delay matrix \mathbf{A} is defined as:

$$\mathbf{A} = \begin{pmatrix} \bar{\mathbf{x}}_0^T \\ \vdots \\ \bar{\mathbf{x}}_{N_t}^T \end{pmatrix} \quad (2)$$

$$\mathbf{C} = \mathbf{A}^T \mathbf{A} = \sum_{k=0}^N \bar{\mathbf{x}}_k \otimes \bar{\mathbf{x}}_k; \quad \mathbf{C} \bar{\mathbf{v}}_k = \mathbf{w}_k^2 \bar{\mathbf{v}}_k, \quad \bar{\mathbf{v}}_k \in \mathbf{R}^M, \quad k = 1, \dots, M \quad (3)$$

then \mathbf{C} is the covariance matrix. Since \mathbf{C} is hermitian by definition, its eigenvectors $\{\bar{\mathbf{v}}_k\}$ form an orthonormal basis in the embedding space. $\{\bar{\mathbf{v}}_k\}$ are usually calculated by using the singular value decomposition (SVD) method, according to which any $M \times N$ matrix \mathbf{A} can be decomposed as:

$$\mathbf{A} = \mathbf{U} \cdot \mathbf{W} \cdot \mathbf{V}^T = \sum_{k=1}^M \mathbf{w}_k \cdot \bar{\mathbf{u}}_k \otimes \bar{\mathbf{v}}_k \quad (4)$$

where

$$\begin{aligned} \mathbf{V} &= (\bar{\mathbf{v}}_1, \dots, \bar{\mathbf{v}}_M), \quad \mathbf{U} = (\bar{\mathbf{u}}_1, \dots, \bar{\mathbf{u}}_M), \\ \mathbf{W} &= \text{diag}(\mathbf{w}_1, \dots, \mathbf{w}_M); \quad \mathbf{U} \cdot \mathbf{U}^T = \mathbf{1}, \quad \mathbf{V} \cdot \mathbf{V}^T = \mathbf{1} \end{aligned}$$

On the other hand when the effective dimension of the system is not known, it is not clear beforehand what number M of delays will provide embedding of the underlying phase space. Broomhead and King [1986] noted using the Lorenz system that the singular spectrum $\{\mathbf{w}_k\}$ of the delay matrix decreases until it reaches a plateau due to the noise in the system. They suggested that M should be the point where the signal turns into noise. However, it turns out that real open systems do not always behave this way. In particular, using VB_S–AL time series Sitnov *et al.* [2000] have shown that in the case of magnetosphere the singular spectrum has well defined power spectral shape that is retained over a wide range of scales with no clear sign of a distinctive noise floor. Hence, it is not always possible to find the appropriate value of M using SVD only. In this work we demonstrate that LLFs themselves can be used for determining the embedding space dimension when applied in an inverse problem manner. That is, if M is considered as a free parameter of the model, then the prediction error can be minimized with respect to this parameter, and the M value which provides the minimum error gives the embedding space dimension.

[13] If the embedding procedure was properly performed, that is, if the attractor of the system was completely unfolded, then the projection of delay vectors on the basis constructed with SVD yields the reconstructed states of the system. These reconstructed states have one-to-one correspondence with the states in the original phase space and thus can be used for predictions of the future evolution of

the system [Farmer and Sidorowich, 1987; Casdagli, 1989, 1992; Sauer, 1993]. For this purpose it is assumed that the underlying dynamics can be described as a nonlinear scalar map $\mathbf{O}_{n+1} = \mathbf{F}(\bar{\mathbf{I}}_n, \bar{\mathbf{O}}_n)$, which relates the current state to the manifestation of the following state, the output time series value at the next time step. The unknown nonlinear function \mathbf{F} is approximated locally for each step of the map by the linear filter:

$$\begin{aligned} \mathbf{O}_{n+1} &\approx \mathbf{F}_0 + (\delta \bar{\mathbf{I}}_n, \delta \bar{\mathbf{O}}_n)^T \cdot \begin{pmatrix} \bar{\alpha} \\ \bar{\beta} \end{pmatrix} \\ &= \mathbf{F}(\bar{\mathbf{I}}_n^C, \bar{\mathbf{O}}_n^C) + \sum_{i=0}^{M_i-1} \alpha_i (\mathbf{I}_{n-i} - \mathbf{I}_{n-i}^C) + \sum_{j=0}^{M_o-1} \beta_j (\mathbf{O}_{n-j} - \mathbf{O}_{n-j}^C) \end{aligned} \quad (5)$$

where $(\bar{\mathbf{I}}_n^C, \bar{\mathbf{O}}_n^C)^T$ is the point about which the expansion is made. The parameters of the filter (α_i , β_j , and \mathbf{F}_0) are calculated using the known data, which is referred to as the training set. The training set is searched for the states similar to the current, that is the states that are closest to it, as measured by the distance in the embedding space defined using the Euclidean metric. These states are referred to as nearest neighbors. LLFs in the form of (5) are also known as local-linear ARMA filters [Detman and Vassiliadis, 1997], since the linear term on the right hand side of (5) is composed of a moving average (MA) part, i.e., the weighted average of preceding inputs, and an autoregressive (AR) part, i.e., the sum of previous outputs.

[14] The zeroth-order term in (5) is a function of the center of expansion, the choice of which is, strictly speaking, ambiguous and should be justified in each particular case. For AE and Dst time series forecasting Price *et al.* [1994] and Valdivia *et al.* [1996] have used the expansion about the origin. Another possible center of expansion can be the reference point, $(\bar{\mathbf{I}}_n, \bar{\mathbf{O}}_n)^T$. For chaotic time series forecasting in autonomous dynamical systems Sauer [1993] suggested that better predictability is achieved when the average state vector of NN nearest neighbors is taken as the center of expansion:

$$\left\langle (\bar{\mathbf{I}}_n, \bar{\mathbf{O}}_n)^T \right\rangle_{\text{NN}} = \frac{1}{\text{NN}} \sum_{k=1}^{\text{NN}} (\bar{\mathbf{I}}_n^k, \bar{\mathbf{O}}_n^k)^T \quad (6)$$

which is also called the center of mass, since (6) is the formula for the center of mass of NN identical particles with coordinates $(\bar{\mathbf{I}}_n^k, \bar{\mathbf{O}}_n^k)$. In this case, if the whole expression (5) is averaged over NN nearest neighbors, the leading term in the expansion \mathbf{F}_0 becomes $\langle \mathbf{O}_{n+1} \rangle_{\text{NN}}$, i.e., the arithmetic average of the outputs corresponding to one step iterated nearest neighbors. The resulting expression for the LLFs takes the form:

$$\begin{aligned} \mathbf{O}_{n+1} &= \langle \mathbf{O}_{n+1} \rangle_{\text{NN}} + \sum_{i=0}^{M_i-1} \alpha_i (\mathbf{I}_{n-i} - \langle \bar{\mathbf{I}}_n \rangle_{\text{NN}}) \\ &+ \sum_{j=0}^{M_o-1} \beta_j (\mathbf{O}_{n-j} - \langle \bar{\mathbf{O}}_n \rangle_{\text{NN}}) \end{aligned} \quad (7)$$

Vassiliadis *et al.* [1995] used local-linear ARMA filters with expansion around the center of mass for both the short and long-term predictions of auroral indices, which gave better

results than the model of Price *et al.* [1994]. It may seem that choosing the center of mass as the expansion center for the filter function is an auxiliary procedure that leads to some increase in the prediction accuracy. However, as we will show later in the paper, in the case of Earth's magnetosphere, and presumably for a large class of nonautonomous real systems, expansion about the center of mass may be the essential element of modeling the system's dynamics with the use of LLFs. It allows a separation of the regular component of the dynamics, stabilizes the prediction algorithm, and provides the basis for modeling the multiscale portion of the dynamics. Moreover, we demonstrate that, as was earlier noted by Kennel and Isabell [1992] for the case of autonomous systems, if the filter function is expanded about the center of mass, the linear terms in equation (7) are irrelevant and can be omitted, as far as long-term predictions are concerned; the best prediction results can be achieved using only the zero-order terms.

[15] When the center of mass is calculated, equation (7) is applied to each of the nearest neighbors. This results in NN linear equations with M unknowns, viz. filter coefficients α_i , β_j and can be expressed as:

$$\mathbf{A}_{\text{NN}} \bar{\mathbf{y}} = \bar{\mathbf{b}} \quad (8)$$

$$\begin{aligned} \bar{\mathbf{y}} &= \begin{pmatrix} \bar{\alpha} \\ \bar{\beta} \end{pmatrix}; \bar{\mathbf{b}} = \begin{pmatrix} \mathbf{O}_{n+1}^1 - \langle \mathbf{O}_{n+1} \rangle_{\text{NN}} \\ \vdots \\ \mathbf{O}_{n+1}^{\text{NN}} - \langle \mathbf{O}_{n+1} \rangle_{\text{NN}} \end{pmatrix}; \\ \mathbf{A}_{\text{NN}} &= \begin{pmatrix} (\bar{\mathbf{I}}_n^1, \bar{\mathbf{O}}_n^1)^T - \left\langle (\bar{\mathbf{I}}_n, \bar{\mathbf{O}}_n)^T \right\rangle_{\text{NN}} \\ \vdots \\ (\bar{\mathbf{I}}_n^{\text{NN}}, \bar{\mathbf{O}}_n^{\text{NN}})^T - \left\langle (\bar{\mathbf{I}}_n, \bar{\mathbf{O}}_n)^T \right\rangle_{\text{NN}} \end{pmatrix} \end{aligned}$$

This system of equation is solved in the least squares sense with use of SVD:

$$\bar{\mathbf{y}} = \mathbf{A}_{\text{NN}}^{-1} \bar{\mathbf{b}} = \sum_{k=1}^{M'} \frac{1}{\mathbf{w}_k^{\text{NN}}} (\bar{\mathbf{b}} \cdot \bar{\mathbf{u}}_k^{\text{NN}}) \bar{\mathbf{v}}_k^{\text{NN}} \quad (9)$$

where $M' \leq M$ is the number of singular values that lie above the prescribed noise floor (tolerance level). Finally, after the filter coefficients are found they are plugged into (7) and then \mathbf{O}_{n+1} is calculated. Combining \mathbf{O}_{n+1} with measured \mathbf{I}_{n+1} and repeating the above steps of the algorithm the next value \mathbf{O}_{n+2} can be evaluated. Thus, local-linear ARMA filters can be used to run the iterative predictions of the system's dynamics.

3. Description of the Data

[16] The LLFs were derived using the correlated database of solar wind and geomagnetic time series compiled by Bargatze *et al.* [1985]. The data are solar wind parameters acquired by IMP 8 spacecraft and simultaneous measurements of auroral indices with resolution of $\tau = 2.5$ min. The database consists of 34 isolated intervals, which contain 42216 points total. Each interval represents isolated auroral

activity preceded and followed by at least 2-hour-long quiet periods ($VB_S \approx 0$, $AL < 50$ nT). Data intervals are arranged in the order of increasing geomagnetic activity. The solar wind convective electric field VB_S is taken as the input of the model. The magnetospheric response to the solar wind activity is represented by the AL index, which is the output of the model. In order to use both VB_S and AL data in joint input–output phase space their time series are normalized to their standard deviations. The prediction accuracy is quantified by normalized mean squared error (NMSE) [Gershensfeld and Weigend, 1993]:

$$\eta = \frac{1}{\sigma_O} \sqrt{\frac{1}{N} \sum_{k=1}^N (\mathbf{O}_k - \hat{\mathbf{O}}_k)^2} \quad (10)$$

Here $k = 1$ to N span the forecasting interval, σ_O is the standard deviation of the original output time series, and $\hat{\mathbf{O}}$ symbol denotes the predicted values. The value $\eta = 1$ corresponds to a prediction of the average.

4. Long-Term Predictions: Global Magnetospheric Dynamics

[17] The modeling of the solar wind–magnetosphere coupling with the use of local-linear ARMA filters yields many new results on the nature of the dynamics of the system. In this section we compare these results with earlier results [Vassiliadis *et al.*, 1995] to isolate the features of LLFs that are important to the long-term forecasting of magnetospheric activity and to look for ways to reconcile the overall predictability with the multiscale aspects of dynamics. For the forecasting of auroral indices Vassiliadis *et al.* [1995] have used ARMA filters with center of mass in the form of (7), taking VB_S as the model input. Applying them to various intervals of the Bargatze database they have shown that the filter response is stable, thus allowing long-term forecasting. The prediction error of their model is minimized at a low number of filter coefficients ($M = 3-6$) that was interpreted as a supporting argument for the low effective dimensionality of the magnetosphere.

[18] Local-linear ARMA filters in the form of (7) are the starting points of the current work as well. The output of the model, AL index, was predicted on the basis on its driver, VB_S . Filters were calculated for both high and low magnetospheric activity periods. In particular, we present calculations for the 31st and the 14th Bargatze intervals.

[19] To define the optimal filter structure for long-term forecasting, the following sequence of steps was performed. First, the testing intervals corresponding to different levels of magnetospheric activity were selected from the database. As for the training set, both input and output data were available for the testing sets. Then, the AL index was predicted for each of the testing intervals using various values of filter parameters, and compared to real data, by calculating the forecasting error (NMSE), for the entire interval. The filter parameters that result in minimal value of NMSE were chosen as optimal. There are three parameters in the ARMA model that can be tuned to minimize NMSE. (1) The number of delays M_i and M_o . For simplicity all calculations were performed for $M_i = M_o = M$. Conceivably, $2M$ also gives a linear hint as to the number of

active degrees of freedom. (2) The number of nearest neighbors (NN), which is used in the calculation of filter coefficients. If NN is comparable to the total number of points in the training set, then the LLF simply becomes a linear filter. (3) The tolerance level, the signal-to-noise ratio, which controls the number of terms in the local singular value spectrum that should be included in the summation in (9).

[20] After considering a wide range of these parameters and calculating filters for different activity intervals we discovered that for long-term predictions formula (7) can be further simplified. For the cases studied here the prediction error minimizes when only zeroth-order terms are taken into account:

$$\mathbf{O}_{n+1} = \langle \mathbf{O}_{n+1} \rangle_{NN} \quad (11)$$

That is, when the value of the output at the next time step is calculated as the arithmetic average of the outputs corresponding to the iterated nearest neighbors of the current state of the system. The forecasting algorithm in this form is very stable and allows iterative predictions of AL time series for several days in a row without any adjustment the filter parameters or reloading the procedure.

[21] Such filters have only two free parameters, NN and M, which should be adjusted to minimize the prediction error. The forecasting of the 31st and the 14th Bargatze intervals, using the filters with the optimized parameters, is presented in Figures 1 and 2. The difference between the real AL data and the model outcome is shown by gray shading. Iterative predictions of the high activity 31st interval were carried out for 2500 min, during which NMSE did not exceed 57%. This result is almost identical to those of Vassiliadis *et al.* [1995, Figure 10] model. However, by using a simplified and therefore more time-efficient algorithm we are able to achieve the same level of accuracy without reloading the procedure after the first 20.8 hours. The forecast of the low-activity interval is also very stable and follows the trend of real data with NMSE equal to 61%.

[22] As can be seen from the plots, the model output closely reproduces the large-scale variations of AL, sometimes failing to capture the most abrupt changes and the sharp peaks. This is intuitively understandable, since the calculation of model outcome reduces to averaging the outputs corresponding to iterated nearest neighbors, the filter output comes inherently smoothed, which results in the observed discrepancy. The higher the number NN of nearest neighbors, the stronger the smoothing and less abrupt the variations of the data can be reproduced by the model. If NN is kept small, then the filter is capable of mimicking rather sharp peaks. However, since the nearest neighbors are identified as the states that have the smallest distance from the current state in the embedding space, an increase in M in this case may result in choosing false nearest neighbors, which leads to prediction error growth. The dependence of prediction error on filter parameters is illustrated by Figure 3, which contains the plots of NMSE as function of NN and M calculated for the 31st and the 14th Bargatze intervals. In both cases NMSE surfaces have similar structures. There is a significant drop in NMSE from 1.0 to 0.6–0.7 when M is increased from 1 (no autoregression) to 3. With further growth of M, NMSE continues to decrease till it reaches

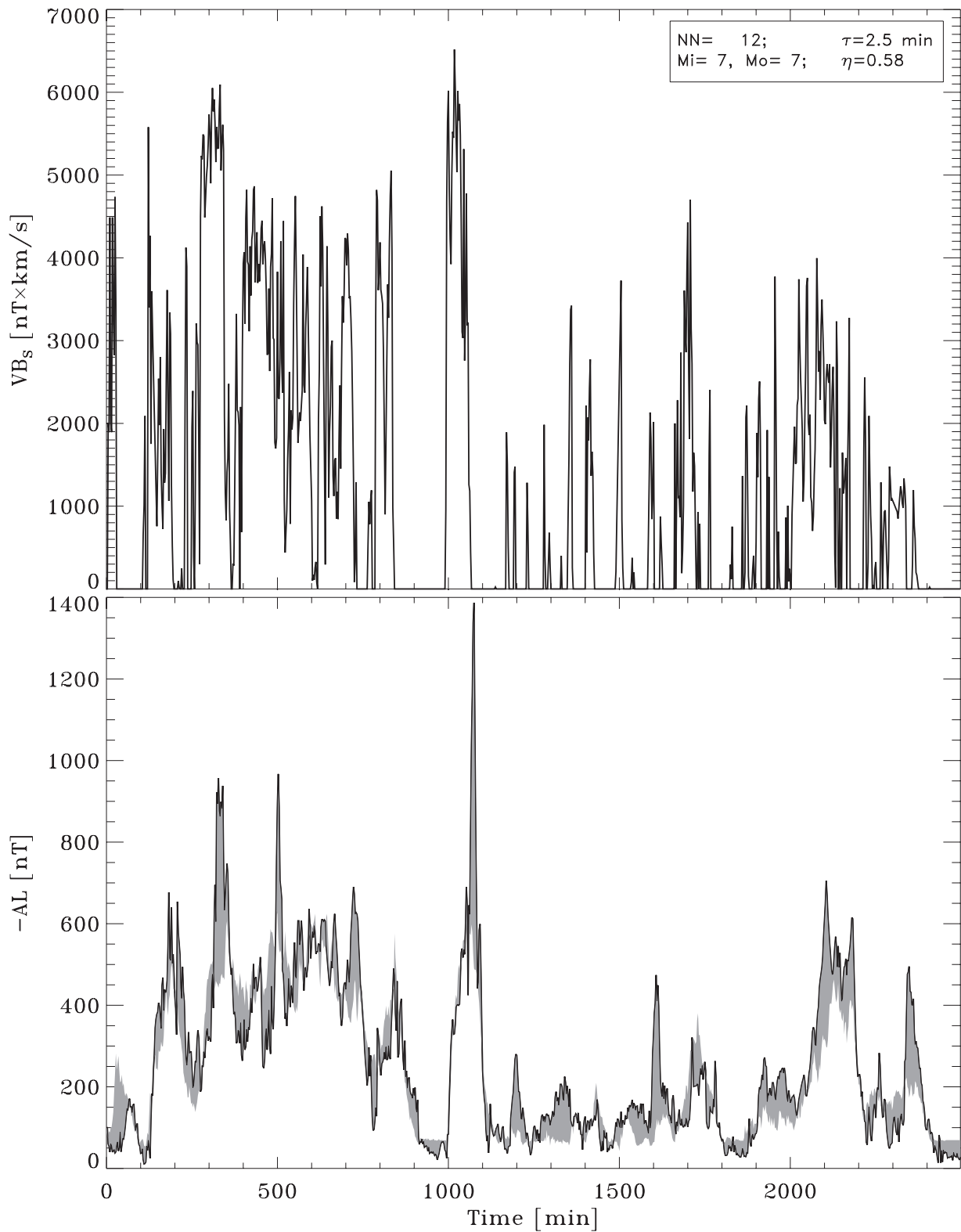


Figure 1. Long-term predictions of AL time series in the 31st Bargatze interval. The model input, VB_s time series, is shown on the upper panel. The bottom panel shows the LLF output together with the observed AL data. The difference between the observed and the predicted time series is shown with gray shading.

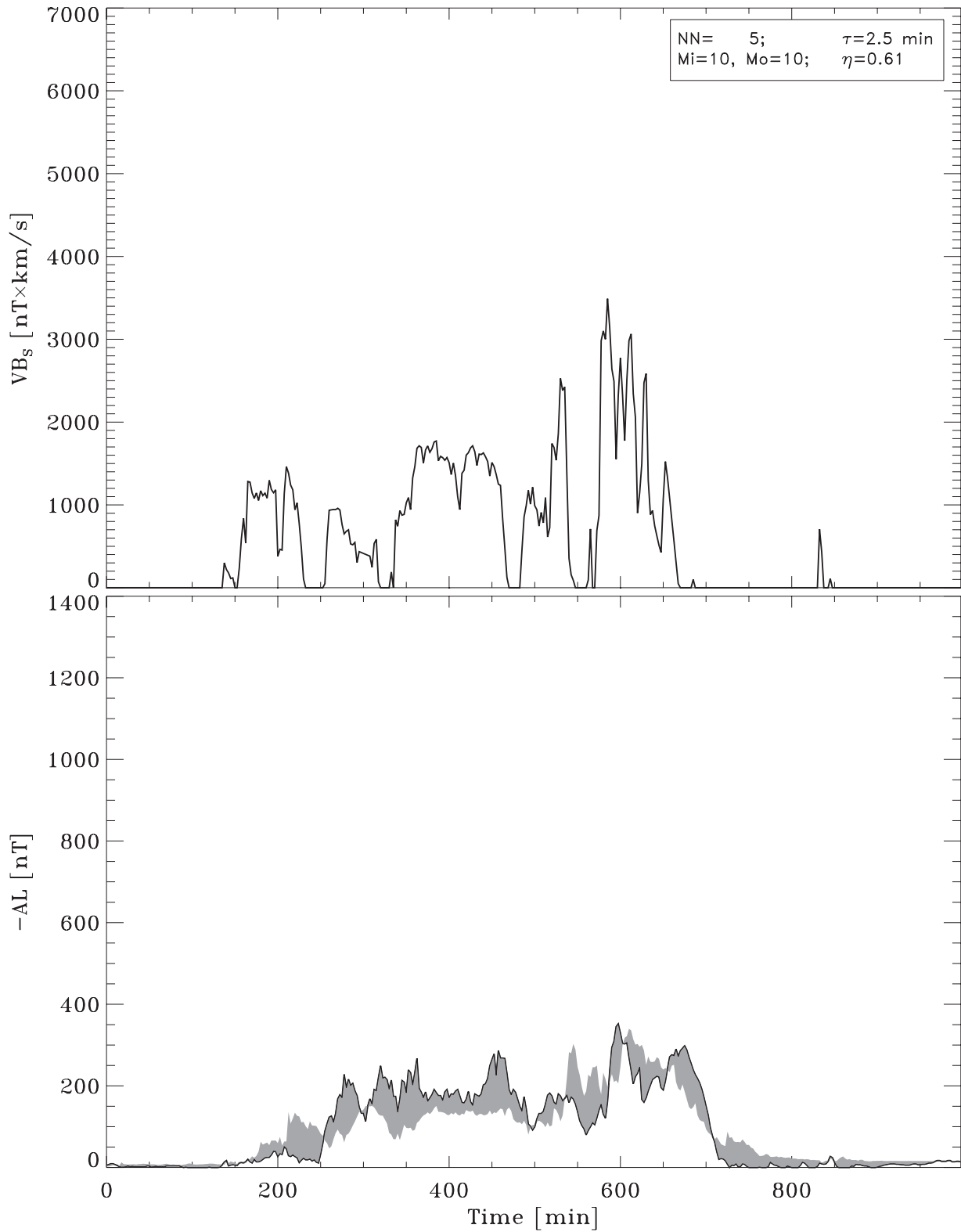


Figure 2. Long-term predictions of AL time series in the 14th Bargatze interval. The model input, VB_s time series, is shown on the upper panel. The bottom panel shows the LLF output together with the observed AL data. The difference between the observed and the predicted time series is shown with gray shading.

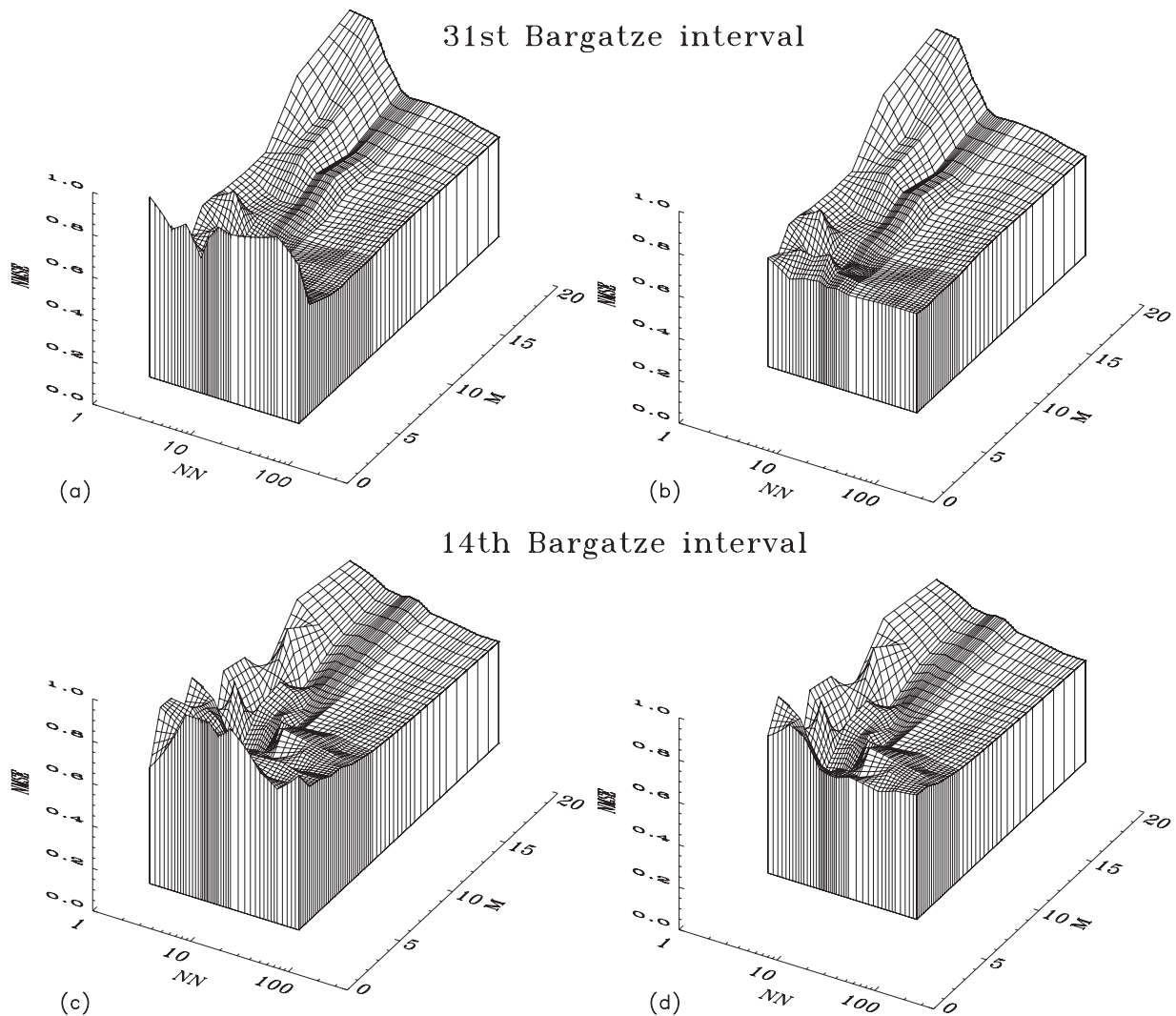


Figure 3. The prediction error (NMSE) of the mean-field model is plotted as a function of the number of nearest neighbors (NN) and the number of delays (M). Error surfaces are plotted for AL predictions in the 31st (a) and 14th (c) Bargatze intervals. To provide a better view on their inner parts, the same surfaces are replotted for the narrower M range ((b) and (d)), starting from $M = 4$ instead of $M = 1$.

its minimum. For the high activity interval the smallest NMSE values are observed for $2M \sim NN = 14$. In the case of low activity, NMSE has several local minima, one of which ($M = 10$, $N = 5$) was chosen for the demonstration run (Figure 2). With further increase in either of filter parameters NMSE starts to grow again. For high NN values it saturates, which indicates that the filter becomes effectively linear. For low NN values, when M increases NMSE grows fast till it reaches 1.0 again. The overall structure of NMSE surfaces shown in Figure 3 is very similar to the error surfaces presented by *Vassiliadis et al.* [1995, Figure 12], except their prediction error reaches its minimum at lower M values (2–3) and higher NN values (~ 30).

[23] If linear terms are included in LLF expression, then the filter response can significantly change, depending on its parameters. If the tolerance level is high, that is a wide range of perturbation scales is taken into account in (9), and $2M \sim NN$ the algorithm becomes unstable and diverges after a few steps. This behavior of the filter outcome can be accounted for by the form of singular value spectrum

obtained from the nearest neighbors matrix. Unlike the global singular spectrum, which has a power law shape, local singular spectrum has a steeper exponential form. The result of local singular spectrum calculations for the 31st Bargatze interval is shown in Figure 4. The spectra were calculated for the set of 80 nearest neighbors at each point of the interval. As can be seen from the plot all spectra are similar in form. The spectra consist of the main exponential part, which is preceded and followed by the shorter intervals of steeper drop. Moreover, singular values calculated for different points of the interval and therefore corresponding to different levels of substorm activity are very similar. This fact may be interpreted as an indication of self-similarity of the attractor that underlies the system dynamics.

[24] In spite of its steepness, the form of the local singular spectra alone does not yield the number of delays M required to embed the underlying phase space. Indeed, the spectra retain their form over the wide range of scales ($10^{-3} < \mathbf{w}_k/\mathbf{w}_0 < 1$) without a noise plateau, and consequently the prescription of *Broomhead and King* [1986]

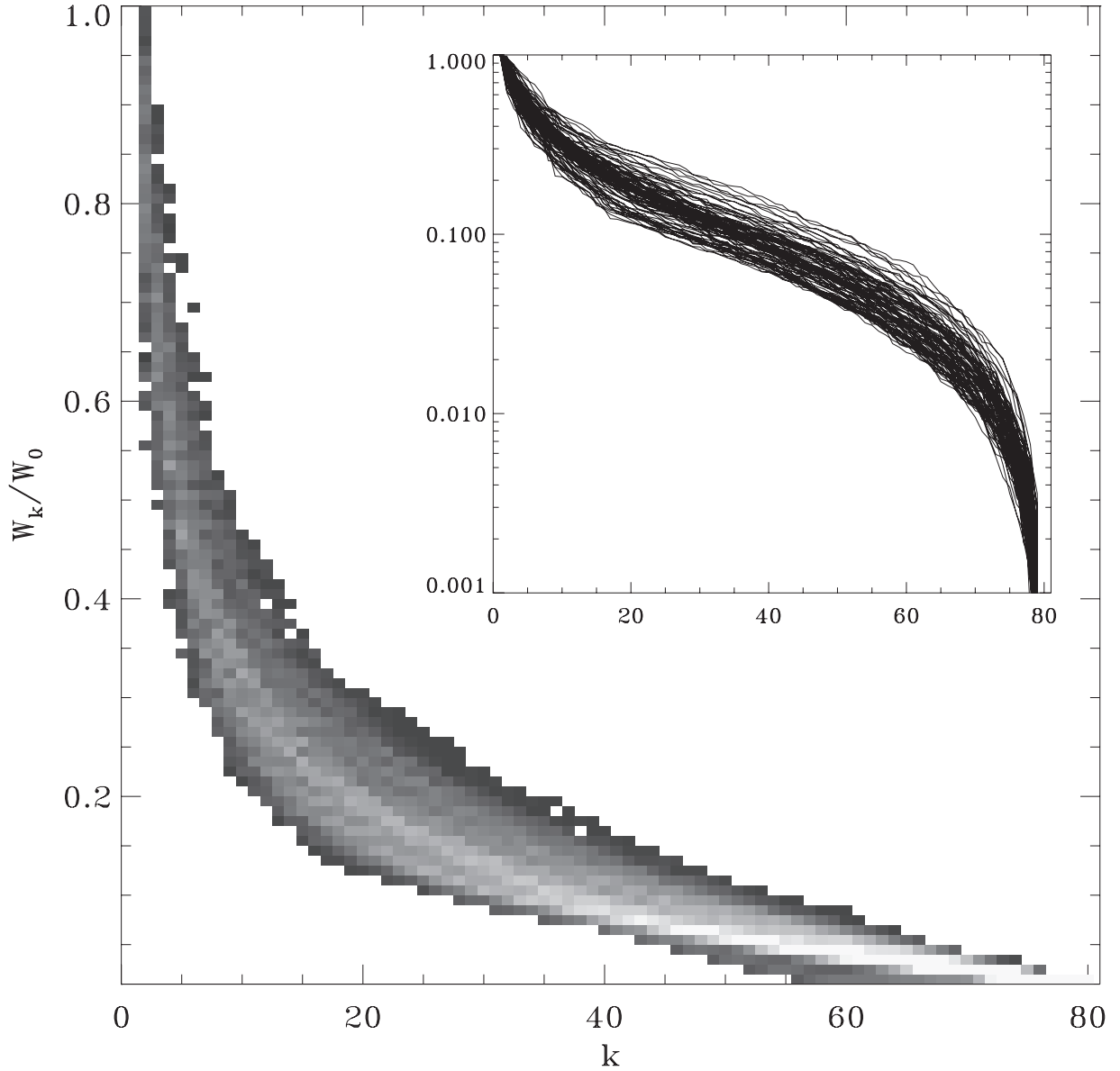


Figure 4. Local singular spectrum (LSS) calculated at each point of the 31st Bargatze interval for $2 \times M = NN = 80$ nearest neighbors matrix. The insert shows LSS in log scale. The color coding on the main plot displays Pdf of singular values.

cannot be used to obtain M . The conventional method used in such cases, i.e., choosing the number of singular values that minimizes the difference:

$$\|A_{NN}(A_{NN}^{-1}\vec{b}) - \vec{b}\| \quad (12)$$

at each step of the iterative predictions, is also not applicable. This follows from the fact that the variance in the estimate of filter coefficients:

$$\sigma(y_j) = \sqrt{\sum_{k=1}^{M'} \left(\frac{1}{w_k^{NN}} (\vec{v}_k^{NN})_j \right)^2} \quad (13)$$

grows exponentially, which results in a divergence of the prediction algorithm for $M' \sim NN$. If M is taken much

greater or much less than NN , the system equation (8) becomes either underdetermined or overdetermined. In the first case, the singular spectra have a different form than the spectra in Figure 4. It has $2M$ gradually decreasing leading values, after which there is a sharp drop to the noise level. Such singular spectra do not lead to the divergence of the prediction algorithm, however, since the equation system for the filter coefficients becomes strongly underdetermined, in most cases the prediction error increases. When the equation (8) is overdetermined the forecasting algorithm also becomes stable, but in this case the filter becomes effectively linear, and prediction error increases. If the tolerance level is low, i.e., only a few leading singular values are included in the summation in (8), then the prediction algorithm becomes stable again. However, the truncation of singular spectrum comes at the cost of information losses and therefore in this case including

linear terms in the model does not improve the predictability. On the contrary in most cases this leads to an increase in forecasting error.

[25] Consequently, for the long-term forecasting of AL time series the linear terms in the expression for conventional local-linear ARMA filters can be omitted. In this case the entire prediction procedure reduces to finding the mean-field response of the system, i.e., the average response of the similar states of the system in the reconstructed input–output phase space. The mean-field model output closely follows the trend of AL data during both high and low magnetospheric activity, reproducing best of all the large-scale variations. Thus, the mean-field model naturally represents the large-scale component of the AL dynamics. Being regular and predictable, it corresponds to the globally coherent features of the magnetospheric dynamics during substorms. Moreover, since the number of delays M is directly related to the effective dimension of the system, the results indicate that the global component of the magnetospheric dynamics has finite dimension.

5. Data Reconstruction: Multiscale Aspects of Magnetospheric Dynamics

[26] The mean-field approach to solar wind–magnetosphere coupling, described in the previous section, provides a framework for modeling the large-scale or global dynamics, for example as represented by AL time series, and for building a framework for space weather forecasting tools. However, the inability to capture the sporadic peaks and abrupt variations in the data may limit the utility of the technique as a space weather forecasting tool.

[27] The inability of the model to yield more accurate forecasts is due to the divergence of the standard prediction algorithm, when a wider range of singular values is considered in the computation of the LLFs. The singular spectrum is analogous to a Fourier spectrum, and the singular values are nothing but the coefficients that weigh the contribution of certain scale perturbations in the observed time series. Thus, the truncation of the singular spectrum, dictated by algorithm stability issues, limits the range of perturbation scales. Moreover, due to the algorithm divergence it is not even clear what this range is, or whether it is finite or not. This issue is of great importance for understanding the dynamical properties of the system as well as for developing more accurate forecasting tools. Indeed, if the range of perturbation scales that are inherent in the observed time series is not finite, then since it is directly related to the number of active dimensions, there is no finite dimensional space that provides a proper embedding for the system. This means that the dynamics of the system is not deterministic and the predictability of its evolution is limited to that of the mean-field model. On the other hand, if the range of perturbation scales is finite and can be somehow determined at each step of the iterative predictions, then including the higher-order terms in filter expression can significantly increase the prediction accuracy.

[28] This is an important issue for space weather forecasting and it can be addressed with use of local-linear ARMA filters in the form given by equation (7). For this purpose, instead of making the iterative predictions of AL

for some testing interval and then minimizing the prediction error by adjusting the filter parameters, and the tolerance level for the whole prediction interval, filters can be used in an inverse problem manner. That is, by comparing the filter outcome with real data at each step of iterative predictions, the number of terms M' of local singular spectrum that gives rise to the observed AL time series (see (9)) can be determined. Presumably, this procedure, which will be referred as data reconstruction, should return the different number M' at each time step. It is expected that in the case of low-dimensional system M' should oscillate around the mean value M^* , which gives the linear estimate of the system dimensionality. However, in the case of a system which has a significant high-dimensional multiscale component, M' should have a sporadic distribution, i.e., M' should be evenly distributed from 1 to $2M$, the total number of input–output embedding space dimensions, no matter how big is M . This indicates that the observed time series consist of perturbations of a wide range of scales.

[29] To elucidate these properties in the case of solar wind–magnetosphere system, we first consider the case of a synchronized Lorenz system, whose dynamical properties are well known. If the X component of one Lorenz attractor is used as a driver for the second Lorenz attractor, then the attractors of both systems synchronize at the following values of parameters: $r = 60.0$, $b = 8/3$, $\sigma = 10$ [Pecora and Carroll, 1990], i.e., no matter what are the initial conditions of the second system after a few steps its trajectory converges to attractor of the driver. Thus, the Y component of the second Lorenz attractor can be considered as an output of the nonautonomous chaotic dynamical system driven by the input, X component of the first Lorenz attractor. The reconstruction of the output by local-linear ARMA filter with $M = 20$ and $NN = 40$ is shown in Figure 5. As can be seen the reconstructed output literally coincides with the actual data, NMSE is only 0.03. The number of terms of the local singular spectrum, which reconstruct the data best at each step of the algorithm, are shown on the third panel of the plot. As expected their distribution function has a narrow peak centered at $M^* = 6$ (the bottom panel of Figure 5), which indicates that we are dealing with a low-dimensional deterministic dynamical system.

[30] To investigate how the distribution of M' changes when the dynamics of the system has two components, one, low dimensional and deterministic, and the other, high dimensional and multiscale, a variation of a synchronized Lorenz system was considered. The second Lorenz attractor was now driven by the superposition of the first Lorenz attractor's X component and $1/f$ noise time series. The reconstruction of such modified Lorenz system is presented in Figure 6. The filter parameters were chosen the same as in the previous example. The NMSE in this case is higher than in the case of the system without noise, but is still very small, 0.21. The existence of a high-dimensional component in both input and output time series leads to dramatic changes in the distribution of the number of singular values chosen from the local spectrum at each step of the reconstruction. Variations in M' now fills the whole range from 1 to $2M$, and its distribution function does not have extrema in this range indicating that these variations are not low dimensional.

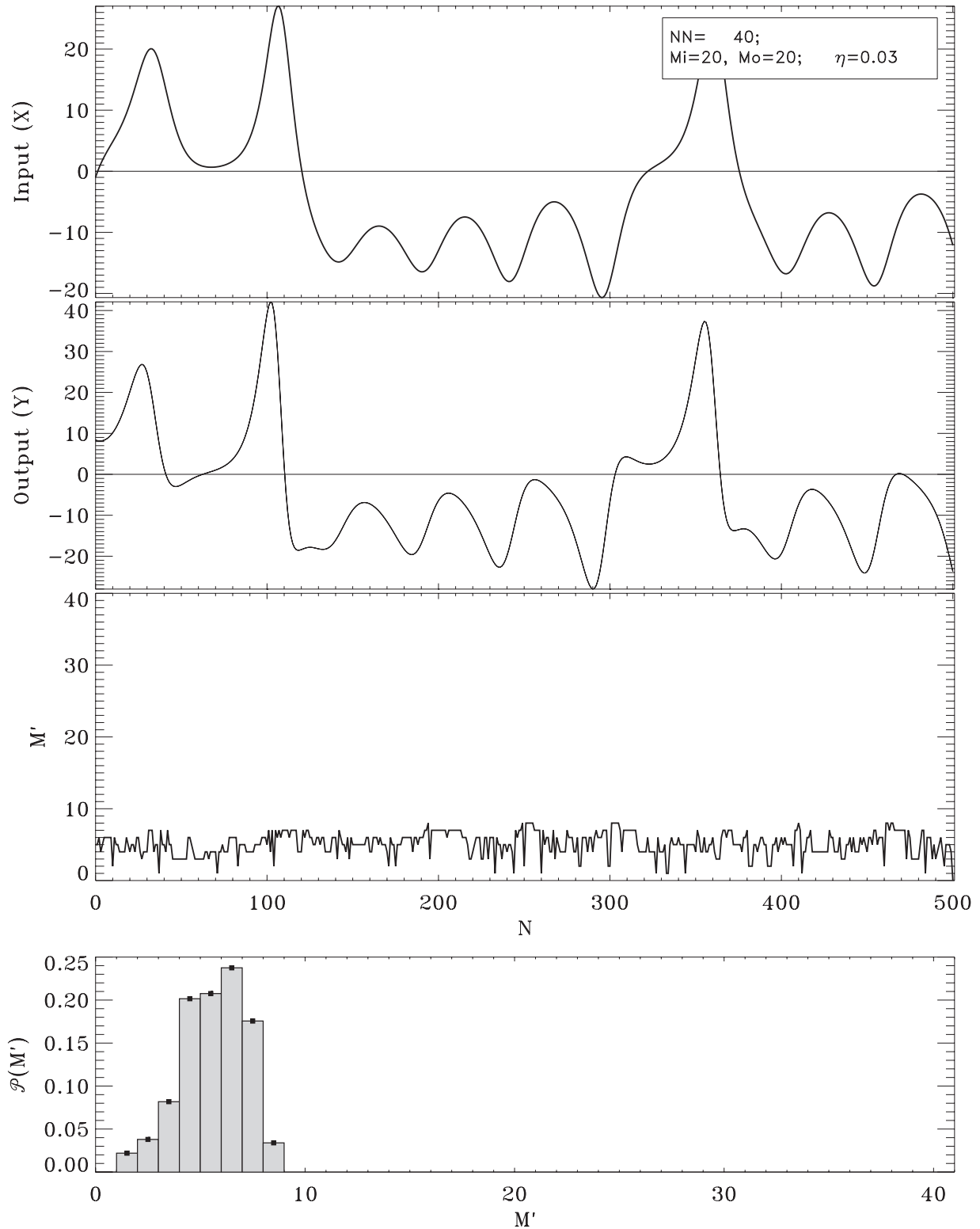


Figure 5. Reconstruction of Y component of synchronized Lorenz attractor from its driver, X component. The model input and output together with the real data are plotted on the two upper panels. Reconstruction error is so small (NMSE = 0.03) that the difference between the reconstructed and the original time series plotted on the second panel is indistinguishable. Distribution function of the number of singular values from the local singular spectrum that provides the best reconstruction is shown on the bottom panel of the plot.

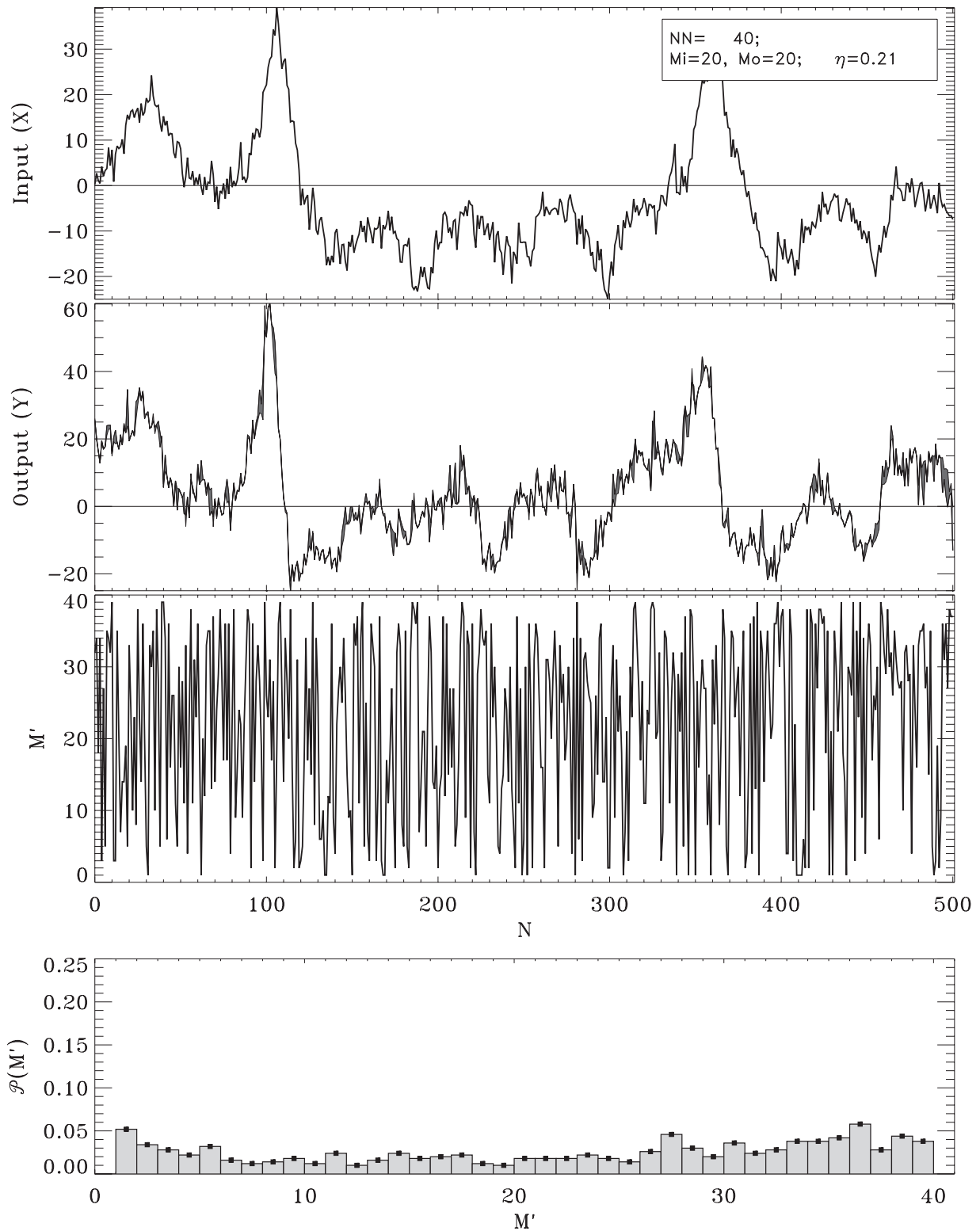


Figure 6. Reconstruction of Y component of synchronized Lorenz attractor contaminated with $1/f$ noise from its driver, X component. The model input and output together with the real data are plotted on the two upper panels. The difference between the observed and the predicted time series is shown with gray shading. Distribution function of the number of singular values from the local singular spectrum that provides the best reconstruction is shown on the bottom panel of the plot.

[31] The results of AL time series reconstruction with the use of local-linear ARMA filter ($M = 20$, $NN = 40$) are shown in Figures 7 and 8. As in the case of predictions both the 31st and the 14th Bargatze intervals are presented. The reconstructed AL follows the real data much closer than the output of the simple mean-field model. The NMSE is very small, 0.14 for the low and 0.18 for the high activity interval, which corresponds to a factor of four decrease compared to the long-term predictions. The distribution functions of the number of singular values required for the best reconstruction of data at each step of the algorithm are shown in the bottom panels of Figures 7 and 8. As can be seen from the plot they are very analogous to M' distribution function obtained for the contaminated Lorenz system, i.e., M' values are distributed uniformly between 1 and $2M$. Moreover, as in the case of Lorenz system this form of M' distribution function holds the same even if the value of M is changed, no matter how big or small. This indicates that except for the low-dimensional coherent component, which is well modeled by the mean-field approach, AL contains a substantial high-dimensional portion, which is also multiscale, i.e., it is build up by the perturbations of a wide range of scales. This also means that the reconstruction error should decrease when M is increased, since it extends the involved range of perturbation scales.

[32] The plots of NMSE calculated for the reconstruction procedure as a function of filter parameters is shown in Figure 9. The error surfaces have a number of features similar to the surfaces obtained for the mean-field model. There is an increase and then saturation of NMSE at high NN values, where the model becomes effectively linear. There is a steep growth of NMSE at high M values when NN is small which is associated with strong indeterminacy of the system given by equation (9). Similarly, there is an abrupt drop of NMSE from 1 to 0.5 when M goes from 1 to 3. However, unlike the mean-field model error NMSE of the reconstruction does not have the local minimum at small M values, after which it starts to grow again with further increase in M . On the contrary, NMSE decreases with an increase of M growth. The error decrease is most substantial along the line $NN = 2M$, where there is a distinct valley in error surfaces. When M reaches 15–20, NMSE saturates, falling as low as 0.15–0.20.

[33] The above results show that the linear terms of local-linear ARMA filters contain the information about the component of AL, which is not captured by the simple mean-field model. This remainder of AL is high dimensional and multiscale in a sense that it contains a wide range of perturbation scales, and its truncation leads to increase in prediction error. Inclusion of the proper number of singular values from the local spectrum can greatly improve the predictability of AL evolution. However, since the distribution of singular values required for the best predictions is uncertain and uniformly fills the whole input–output state space, no matter what is its dimensionality, it is not clear yet what prescription will give the proper number of singular values at each prediction step.

6. Conclusions

[34] In this paper the LLF approach to the magnetospheric dynamics modeling, first proposed by *Prichard*

and *Price* [1992], *Price and Prichard* [1993], and *Price et al.* [1994] and later elaborated by *Vassiliadis et al.* [1995], has been used to study the global and multiscale aspects of the solar wind–magnetosphere coupling during substorms. The filters which were derived from the reconstructed input–output phase space of the system using VB_S time series as the input and AL time series as the output of the model were found to reveal both globally coherent and multiscale features of magnetospheric dynamics during substorms. Our main results can be separated in two parts.

[35] First, after considering a wide range of filter parameters it is found that for the purpose of long-term forecasting the conventional formula for local-linear ARMA filters can be greatly simplified. The filter response can be estimated in a mean-field fashion, i.e., by averaging outputs corresponding to similar states of the system in the reconstructed phase space. The mean-field method can yield accurate iterative predictions of AL time series for several days in a row during periods of both high and low magnetospheric activity, capturing best of all the large-scale variations of data. The mean-field model output naturally distinguishes the component of the AL time series, which is regular and predictable and therefore corresponds to the large-scale coherent portion of magnetospheric dynamics during substorms. This result makes the forecasting of the global behavior simpler and easier to implement compared with earlier studies.

[36] It is interesting that similar results have been already reported for autonomous systems by *Pikovsky* [1986] and *Kennel and Isabell* [1992]. In the context of magnetospheric research *Vassiliadis et al.* [1995] used the averaging over nearest neighbors as one of the elements of their ARMA filters together with the Taylor expansion around the center of mass. We have shown that the latter expansion is unnecessary in the specific case of input–output (VB_S , AL) data set, and the global deterministic component of the magnetospheric dynamics can be captured by the straightforward local averaging of the training set in the embedding space.

[37] Second, our results elucidate the multiscale constituent of the solar wind–magnetospheric activity. We have found that the portion of AL, which is not captured by simple mean-field model, can be still reproduced with local-linear ARMA filters if the number of terms in the local singular spectrum is optimized by comparing the model output with real data at each step of predictions. It turns out that this remainder of AL dynamics contains perturbations of a wide range of scales, has high dimensionality, and therefore corresponds to the multiscale features of the magnetospheric dynamics during substorms. If the proper number of singular values is used in the calculation of linear terms of local-linear ARMA filters, then the predictability of AL can be increased by a factor of four or more compared to the mean-field model. This gives an attractive prospect for developing reliable space weather forecasting tools. However, since the distribution function of the optimal number of singular values uniformly fills the whole embedding space, no matter what its dimensionality is, it is not clear yet how to choose the proper number in advance. It is not even clear that such a procedure is in general possible, since this multiscale remainder shares a number of properties with colored noise.

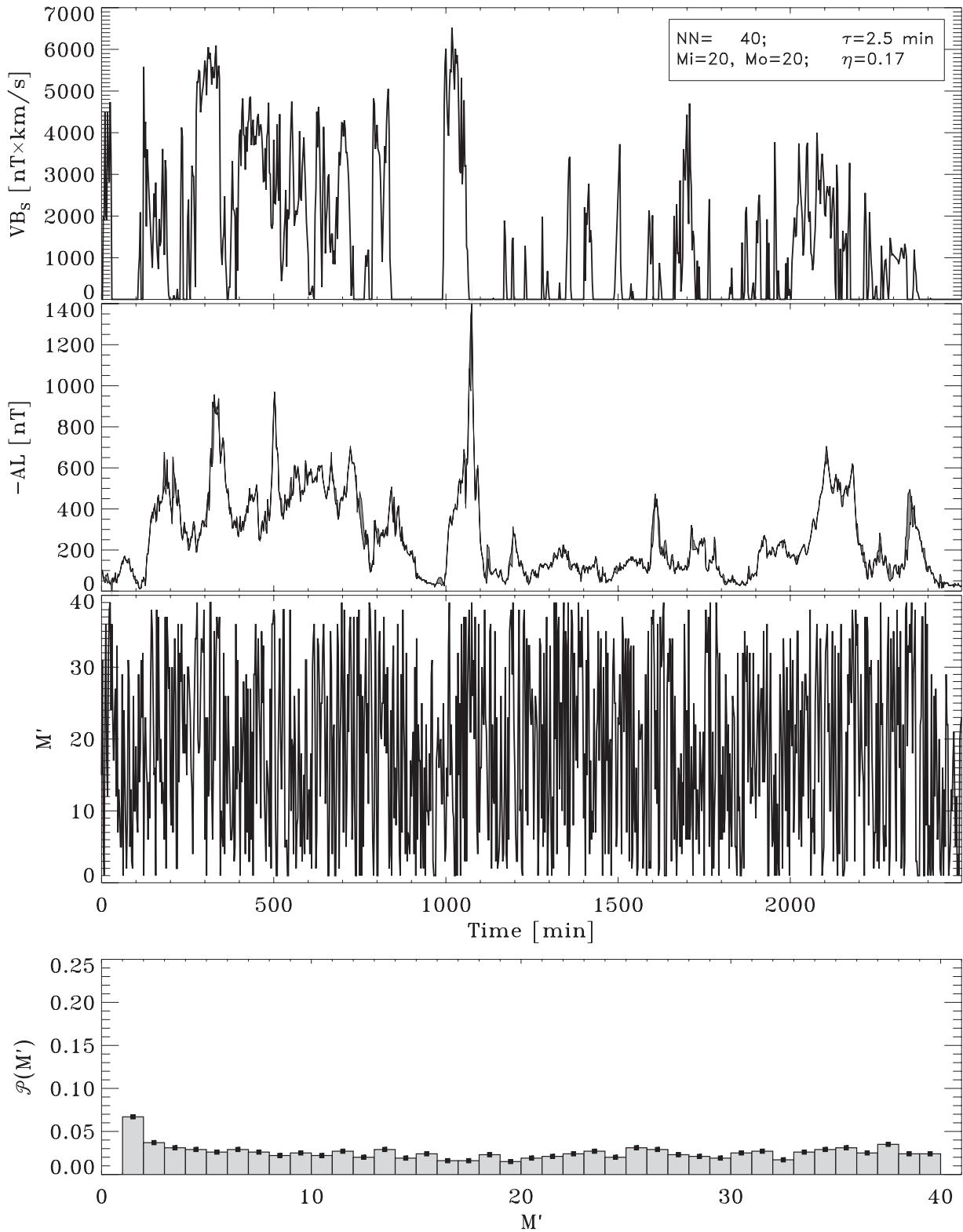


Figure 7. Reconstruction of AL time series in the 31st Bargatze interval. The model input and output together with the observed AL data are plotted on the two upper panels. The difference between the observed and the predicted time series is shown with gray shading. Distribution function of the number of singular values from the local singular spectrum that provides the best reconstruction is shown on the bottom panel of the plot.

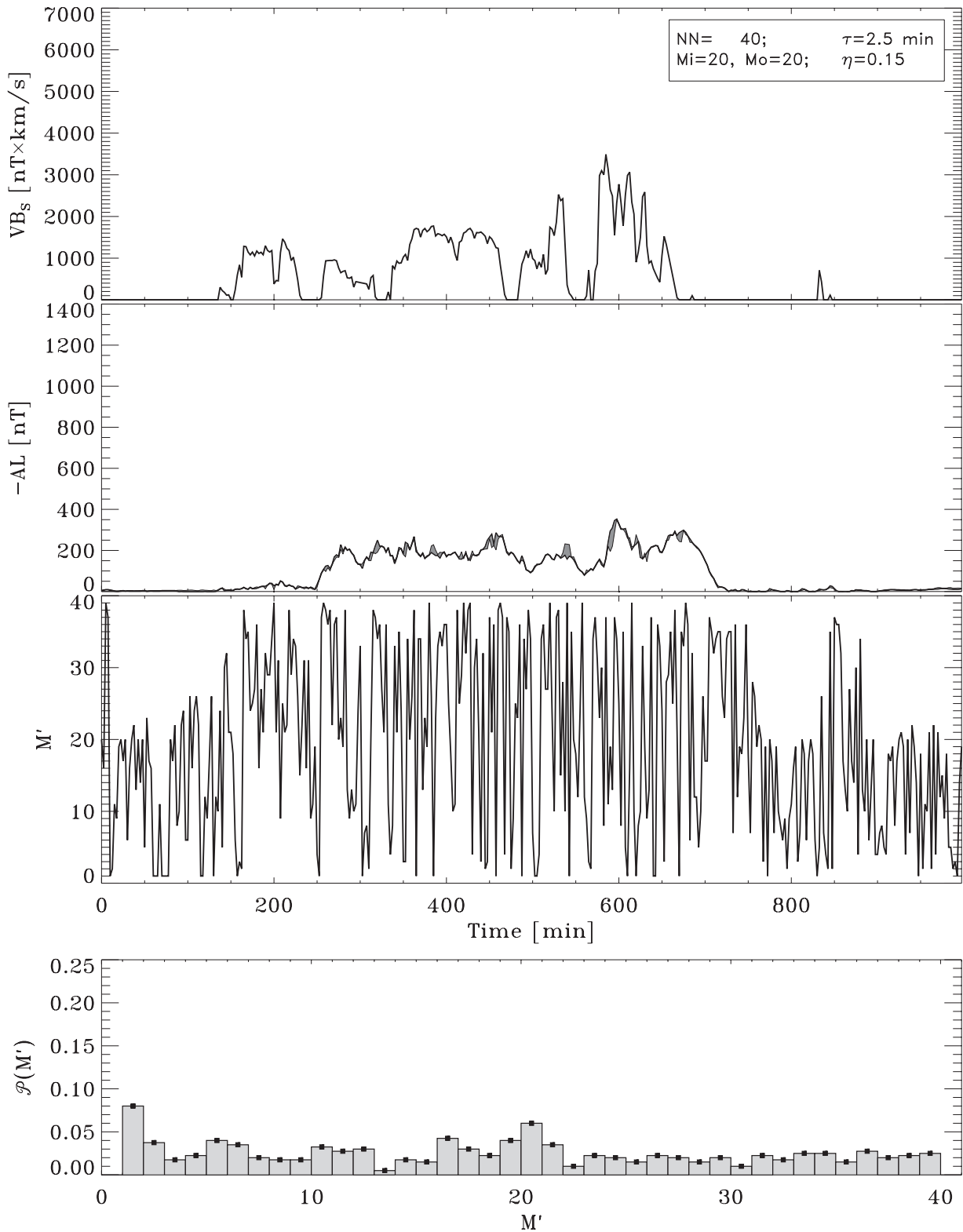


Figure 8. Reconstruction of AL time series in the 14th Bargatze interval. The model input and output together with the observed AL data are plotted on the two upper panels. The difference between the observed and the predicted time series is shown with gray shading. Distribution function of the number of singular values from the local singular spectrum that provides the best reconstruction is shown on the bottom panel of the plot.

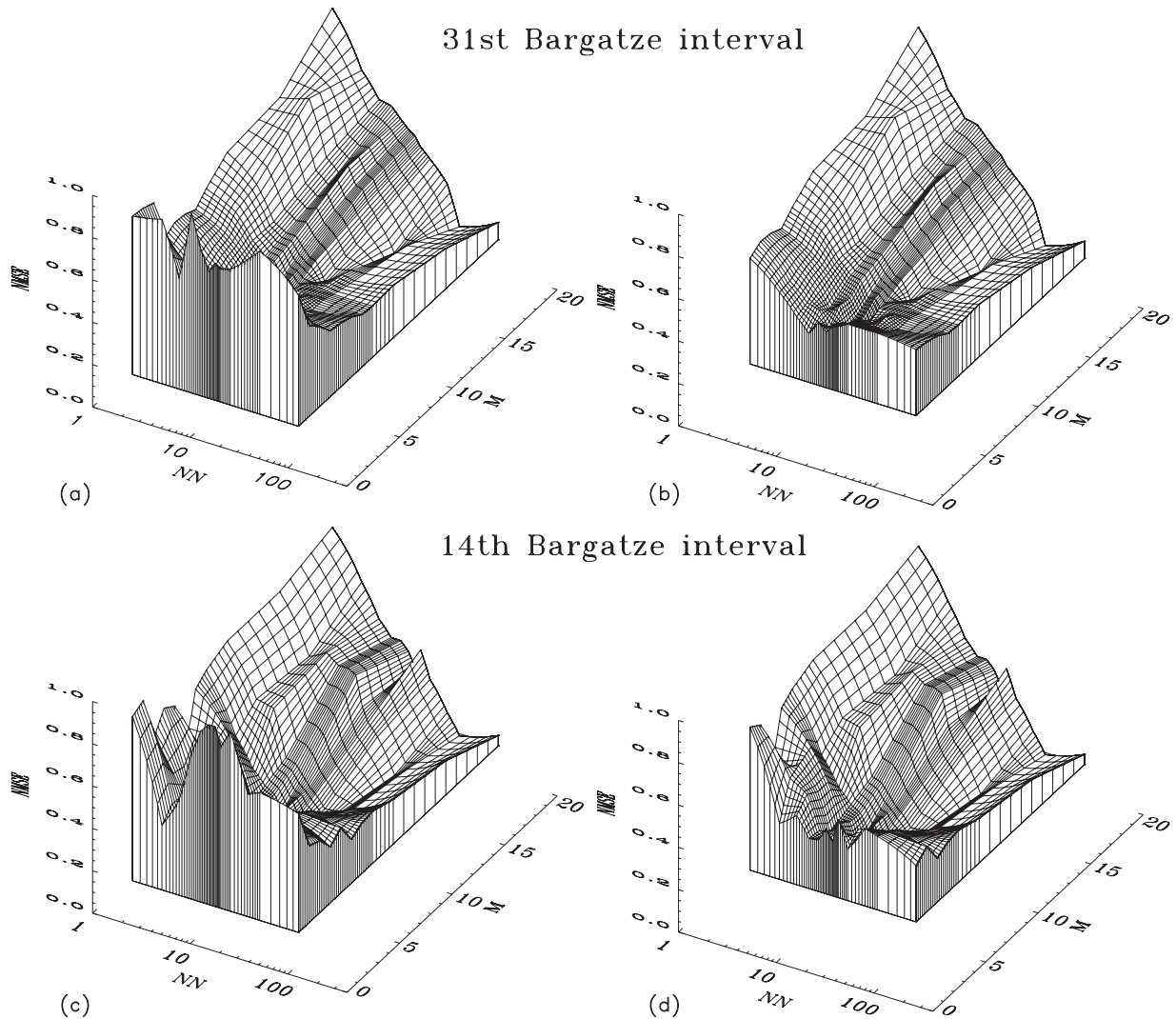


Figure 9. The reconstruction error (NMSE) is plotted as a function of the number of nearest neighbors (NN) and the number of delays (M). Error surfaces are plotted for AL reconstruction in the 31st (a) and 14th (c) Bargatze intervals. To provide a better view on their inner parts, the same surfaces are replotted for the narrower M range ((b) and (d)), starting from $M = 4$ instead of $M = 1$.

[38] From the irregular behavior of LLF linear terms it is also evident that the multiscale properties of magnetospheric dynamics have different nature from those of simple dynamical systems like synchronized Lorenz attractor, which reconcile scale invariance with low dimensionality due to the fractal nature of their attractors. Linear terms of LLF constructed for such systems are regular which reflects the existence of smooth manifold that contains the dynamic attractor on arbitrary small scales. In this case including higher-order terms into LLF model leads to an increase in predictability [e.g., Sauer, 1993]. The sporadic behavior of LLF linear terms derived for solar wind–magnetosphere system indicates that on small scales there is no smooth manifold in the embedding space of arbitrary high dimensionality that would contain the trajectories of system. This also means that the multiscale portion of time the series not captured by the mean-field model has infinite or high dimensionality.

[39] Thus, the input–output VB_S –AL data with use of LLFs suggests that the solar wind–magnetosphere coupling

during substorms as observed in AL time series can be summarized by the following dynamic equation:

$$\frac{d}{dt} \mathbf{AL}(t) = \langle \mathbf{AL} \rangle_{NN} + \varepsilon(\bar{\mathbf{A}}\bar{\mathbf{L}}, \bar{\mathbf{V}}\bar{\mathbf{B}}_s, t) \quad (14)$$

where the first term on the right side is the mean-field term, derived by the averaging over reconstructed input–output phase space, which describes the global coherent portion of magnetospheric dynamics, while the second term is responsible for the high-dimensional multiscale constituent.

[40] The above data-derived picture of the magnetospheric activity during substorms in response to the solar wind driving is consistent with the earlier results obtained on the basis of the global singular spectrum analysis of VB_S –AL data [Sitnov *et al.*, 2000, 2001; Sharma *et al.*, 2001]. It was found in particular that the global and multiscale properties of magnetospheric dynamics are organized in a manner similar to conventional phase transitions [e.g., Stanley, 1971] with the largest-scale phenomena resembling

first-order phase transitions in the mean-field approximation, while the multiscale constituent having properties of second-order transitions near the critical point. The first-order transition picture of the magnetosphere was obtained in the three leading principal components corresponding to the largest eigenvalues of the correlation matrix with additional local averaging in that 3D space. The average dynamics of the magnetosphere is then similar to the regular motion on a folded surface like the “temperature–pressure–density” diagram of dynamical phase transitions [e.g., Gunton *et al.*, 1983] or the cusp catastrophe manifold [Lewis, 1991]. Our present results strongly support such a description of the mean-field picture. On the other hand, the results of the global singular spectrum analysis suggest that the multiscale constituent of the magnetospheric activity may be neither a colored noise independent of the solar wind properties as suggested in the models of magnetospheric turbulence [e.g., Borovsky *et al.*, 1993, 1997] and SOC [e.g., Consolini, 1997; Chapman *et al.*, 1998; Uritsky and Pudovkin, 1998; Lui *et al.*, 2000], nor a direct reflection of the appropriate multiscale solar wind properties as suggested by Freeman *et al.* [2000]. It can rather be viewed as the multiscale response involving both input and output parameters as is reflected by input–output critical exponents similar to those of the second-order phase transitions [Sitnov *et al.*, 2001]. Therefore, further improvement in the predictability may be achieved by a combination of the dynamical description for the global component and a statistical approach for the multiscale component, by studying its correlation with the solar wind input.

[41] **Acknowledgments.** We thank D. Vassiliadis for many fruitful discussions. The research is supported by NSF grants ATM-0001676 and ATM-0119196 and NASA grant NAG5-1101.

References

- Abarbanel, H. D., R. Brown, J. J. Sidorovich, and T. S. Tsimring, The analysis of observed chaotic data in physical systems, *Rev. Mod. Phys.*, **65**, 1331, 1993.
- Angelopoulos, V., T. Mukai, and S. Kokubun, Evidence for intermittency in Earth's plasma sheet and implications for self-organized criticality, *Phys. Plasmas*, **6**, 4161, 1999.
- Bak, P., C. Tang, and K. Wiesenfeld, Self-organized criticality: An explanation of $1/f$ noise, *Phys. Rev. Lett.*, **59**, 381, 1987.
- Bargatze, L. F., D. N. Baker, R. L. McPherron, and E. W. Hones, Magnetospheric impulse response for many levels of geomagnetic activity, *J. Geophys. Res.*, **90**, 6387, 1985.
- Borovsky, J. E., R. J. Nemzek, and R. D. Belian, The occurrence rate of magnetospheric-substorm onsets: Random and periodic substorms, *J. Geophys. Res.*, **98**, 3807, 1993.
- Borovsky, J. E., R. C. Elphic, H. O. Funsten, and M. F. Thomsen, The Earth's plasma sheet as a laboratory for flow turbulence in high- β MHD, *J. Plasma Phys.*, **57**, 1, 1997.
- Broomhead, D. S., and G. P. King, Extracting qualitative dynamics from experimental data, *Physica D*, **20**, 217, 1986.
- Casdagli, M., Nonlinear prediction of chaotic time series, *Physica D*, **35**, 335, 1989.
- Casdagli, M., A dynamical approach to modeling input–output systems, in *Nonlinear Modeling and Forecasting*, edited by M. Casdagli and S. Eubank, p. 265, Addison-Wesley-Longman, Reading, Mass., 1992.
- Chakrabarti, B. K., and M. Acharyya, Dynamic transitions and hysteresis, *Rev. Mod. Phys.*, **71**, 847, 1999.
- Chang, T., Multiscale intermittent turbulence in the magnetotail, in *SUBSTORMS-4*, edited by S. Kokubun and Y. Kamide, p. 431, Terra Sci., Tokyo, 1998.
- Chang, T., Self-organized criticality, multi-fractal spectra, sporadic localized reconnections and intermittent turbulence in the magnetotail, *Phys. Plasmas*, **6**, 4137–4145, 1999.
- Chapman, S. C., N. W. Watkins, R. O. Dendy, P. Helander, and G. Rowlands, A simple avalanche model as an analogue for magnetospheric activity, *Geophys. Res. Lett.*, **25**, 2397, 1998.
- Consolini, G., Sandpile cellular automata and magnetospheric dynamics, in *Proceeding of the 8th GIFCO Conference, Cosmic Physics in the Year 2000: Scientific Perspectives and New Instrumentation*, 8–10 April 1997, edited by S. Aiello *et al.*, Soc. Ital. di Fis., Bologna, Italy, pp. 123–126, 1997.
- Consolini, G., M. F. Marcucci, and M. Candidi, Multifractal structure of auroral electrojet index data, *Phys. Rev. Lett.*, **76**, 4082, 1996.
- Detman, T. R., and D. Vassiliadis, Review of techniques of the magnetic storm forecasting, in *Magnetic Storms, Geophys. Monogr. Ser.*, vol. 98, edited by B. T. Tsurutani *et al.*, pp. 253–266, AGU, Washington, D. C., 1997.
- Farmer, J. D., and J. J. Sidorowich, Predicting chaotic time series, *Phys. Rev. Lett.*, **59**, 845, 1987.
- Freeman, M. P., N. W. Watkins, and D. J. Riley, Evidence for solar wind origin of the power law burst lifetime distribution of the AE indices, *Geophys. Res. Lett.*, **27**, 1087, 2000.
- Gershenfeld, N. A., and A. S. Weigend, The future of time series: Learning and understanding, in *Time Series Prediction: Forecasting the Future and Understanding the Past, Santa Fe Inst. Stud. in the Sci. of Complexity XV*, edited by A. S. Weigend and N. A. Gershenfeld, pp. 1–70, Addison-Wesley-Longman, Reading, Mass., 1993.
- Grassberger, P., and I. Procaccia, Measuring the strangeness of strange attractors, *Physica D*, **9**, 189, 1983.
- Gunton, J. D., M. S. Miguel, and P. S. Sahni, The dynamics of first-order phase transitions, in *Phase Transitions, Volume 8*, p. 267, Academic, San Diego, Calif., 1983.
- Hohenberg, P. C., and B. I. Halperin, Theory of dynamic critical phenomena, *Rev. Mod. Phys.*, **49**, 435, 1977.
- Ieda, A., S. Mashida, T. Mukai, Y. Saito, T. Yamamoto, A. Nishida, T. Terasawa, and S. Kokubun, Statistical analysis of the plasmoid evolution with Geotail observations, *J. Geophys. Res.*, **103**, 4453, 1998.
- Kennel, M. B., and S. Isabell, Method to distinguish possible chaos from colored noise and to determine embedding parameters, *Phys. Rev. A*, **46**, 3111, 1992.
- Klimas, A. J., D. N. Baker, D. A. Roberts, D. H. Fairfield, and J. Buchner, A nonlinear dynamical analogue model of geomagnetic activity, *J. Geophys. Res.*, **97**, 12,253, 1992.
- Klimas, A. J., D. Vassiliadis, D. A. Roberts, and D. N. Baker, The organized nonlinear dynamics of the magnetosphere (an invited review), *J. Geophys. Res.*, **101**, 13,089, 1996.
- Klimas, A. J., J. A. Valdivia, D. Vassiliadis, D. N. Baker, M. Hesse, and J. Takalo, Self-organized criticality in the substorm phenomenon and its relation to localized reconnection in the magnetospheric plasma sheet, *J. Geophys. Res.*, **105**, 18,765, 2000.
- Lewis, Z. V., On the apparent randomness of substorm onset, *Geophys. Res. Lett.*, **18**, 1627, 1991.
- Lui, A. T. Y., A. C. Chapman, K. Liou, P. T. Newell, C. I. Meng, M. Brittner, and G. K. Parks, Is the dynamic of magnetosphere an avalanching system?, *Geophys. Res. Lett.*, **27**, 911, 2000.
- Nagai, T., M. Fujimoto, Y. Saito, S. Mashida, T. Terasawa, R. Nakamura, T. Yamamoto, T. Mukai, A. Nishida, and S. Kokubun, Structure and dynamics of magnetic reconnection for substorm onsets with Geotail observations, *J. Geophys. Res.*, **103**, 4419, 1998.
- Nagel, S. R., Instabilities in a sandpile, *Rev. Mod. Phys.*, **64**, 321–325, 1992.
- Ohtani, S., T. Higuchi, A. T. Lui, and K. Takahashi, Magnetic fluctuations associated with tail current disruption: Fractal analysis, *J. Geophys. Res.*, **100**, 19,135, 1995.
- Packard, N., J. Crutchfield, D. Farmer, and R. Shaw, Geometry from a time series, *Phys. Rev. Lett.*, **45**, 712, 1980.
- Pecora, L. M., and T. L. Carroll, Synchronization in chaotic systems, *Phys. Rev. Lett.*, **64**, 821, 1990.
- Petrukovich, A. A., *et al.*, Two spacecraft observations of a reconnection pulse during an auroral breakup, *J. Geophys. Res.*, **103**, 47, 1998.
- Pikovskiy, A., Noise filtering in the discrete time dynamical systems, *Sov. J. Commun. Technol. Electron.*, **31**, 911, 1986.
- Price, C. P., and D. Prichard, The nonlinear response of the magnetosphere: 30 October 1978, *Geophys. Res. Lett.*, **20**, 771, 1993.
- Price, C. P., D. Prichard, and J. E. Bischoff, Non-linear input/output analysis of the auroral electrojet index, *J. Geophys. Res.*, **99**, 13,227, 1994.
- Prichard, D., and C. P. Price, Is the AE index the result of nonlinear dynamics?, *Geophys. Res. Lett.*, **20**, 2817, 1992.
- Prichard, D., J. E. Borovsky, P. M. Lemons, and C. P. Price, Time dependence of substorm recurrence: An information theoretic analysis, *J. Geophys. Res.*, **101**, 15,359, 1996.
- Sauer, T., Time series prediction by using delay coordinate embedding, in *Time Series Prediction: Forecasting the Future and Understanding the Past, Santa Fe Inst. Stud. in the Sci. of Complexity XV*, edited by A. S.

- Weigend and N. A. Gershenfeld, pp. 175–193, Addison-Wesley-Longman, Reading, Mass., 1993.
- Sauer, T., J. A. Yorke, and M. Casdagli, Embedology, *J. Stat. Phys.*, 65, 579, 1991.
- Sharma, A. S., Assessing the magnetosphere's nonlinear behavior: Its dimension is low, its predictability high (US National Report to IUGG, 1991–1994), *Rev. Geophys. Suppl.*, 33, 645–650, 1995.
- Sharma, A. S., D. Vassiliadis, and K. Papadopoulos, Reconstruction of low dimensional magnetospheric dynamics by singular spectrum analysis, *Geophys. Res. Lett.*, 20, 335, 1993.
- Sharma, A. S., M. I. Sitnov, and K. Papadopoulos, Substorms as nonequilibrium transitions in the magnetosphere, *J. Atmos. Sol. Terr. Phys.*, 63, 1399, 2001.
- Sitnov, M. I., A. S. Sharma, K. Papadopoulos, D. Vassiliadis, J. A. Valdivia, A. J. Klimas, and D. N. Baker, Phase transition-like behavior of the magnetosphere during substorms, *J. Geophys. Res.*, 105, 12,955, 2000.
- Sitnov, M. I., A. S. Sharma, K. Papadopoulos, and D. Vassiliadis, Modeling substorm dynamics of the magnetosphere: From self-organization and self-criticality to nonequilibrium phase transitions, *Phys. Rev. E.*, 65, 16,116, 2001.
- Smith, A. J., M. P. Freeman, and G. D. Reeves, Postmidnight VLF chorus events, a substorm signature observed at the ground near $L = 4$, *J. Geophys. Res.*, 101, 24,641, 1996.
- Stanley, H. E., *Introduction to Phase Transition and Critical Phenomena*, Oxford Univ. Press, New York, 1971.
- Takalo, J., J. Timonen, and H. Koskinen, Correlation dimension and affinity of AE data and bicolored noise, *Geophys. Res. Lett.*, 20, 1527, 1993.
- Takalo, J., J. Timonen, and H. Koskinen, Properties of AE data and bicolored noise, *J. Geophys. Res.*, 99, 13,239, 1994.
- Takalo, J., J. Timonen, A. J. Klimas, J. A. Valdivia, and D. Vassiliadis, Nonlinear energy dissipation in a cellular automation magnetotail model, *Geophys. Res. Lett.*, 26, 1813, 1999.
- Takens, F., Detecting strange attractors in fluid turbulence, in *Dynamical Systems and Turbulence*, edited by D. Rand and L. S. Young, pp. 366–381, Springer-Verlag, New York, 1981.
- Theiler, J., Some comments on the correlation dimension of $1/f^\alpha$ noise, *Phys. Lett. A*, 155, 480, 1991.
- Tsurutani, B. T., M. Sugiura, T. Iyemori, B. E. Goldstein, W. D. Gonzalez, S. I. Akasofu, and E. J. Smith, The nonlinear response of AE to the IMF Bs driver: A spectral break at 5 hours, *Geophys. Res. Lett.*, 17, 279, 1990.
- Uritsky, V. M., and M. I. Pudovkin, Low frequency $1/f$ -like fluctuations of the AE-index as a possible manifestation of self-organized criticality in the magnetosphere, *Ann. Geophys.*, 16(12), 1580, 1998.
- Valdivia, J. A., A. S. Sharma, and K. Papadopoulos, Prediction of magnetic storms with nonlinear dynamical models, *Geophys. Res. Lett.*, 23, 2899, 1996.
- Vassiliadis, D., A. S. Sharma, T. E. Eastman, and K. Papadopoulos, Low dimensional chaos in magnetospheric activity from AE time series, *Geophys. Res. Lett.*, 17, 1841, 1990.
- Vassiliadis, D., A. J. Klimas, D. B. Baker, and D. A. Roberts, A description of the solar wind–magnetosphere coupling based on nonlinear filters, *J. Geophys. Res.*, 100, 3495, 1995.
- Vespignani, A., and S. Zapperi, How self-organized criticality works: A unified mean-field picture, *Phys. Rev. E*, 57, 6345, 1998.
- Watkins, N. W., S. C. Chapman, R. O. Dendy, and G. Rowlands, Robustness of collective behaviour in strongly driven avalanche models: Magnetospheric implications, *Geophys. Res. Lett.*, 26, 2617, 1999.
- Zheng, B., M. Schulz, and S. Trimper, Deterministic equations of motion and dynamic critical phenomena, *Phys. Rev. Lett.*, 82, 1891, 1999.

K. Papadopoulos, A. S. Sharma, M. I. Sitnov, and A. Y. Ukhorskiy, Department of Physics, University of Maryland at College Park, College Park, MD, USA.